Dielectronic recombination in C^{3+} above and below the ionization threshold

M. S. Pindzola, S. D. Loch, and F. Robicheaux
Department of Physics, Auburn University, Auburn, Alabama, USA
(Received 8 February 2011; published 8 April 2011)

Low-order relativistic perturbation-theory calculations are carried out for dielectronic recombination cross sections for C^{3+} above and below the ionization threshold. Cross-sectional calculations are made for the 38 levels of the $1s^22p4l$ resonance configurations that lie within ± 1.0 eV of the ionization threshold. The below-threshold calculations predict an unobserved strong resonance feature and provide a guide for future experiments.

DOI: 10.1103/PhysRevA.83.042705 PACS number(s): 34.80.Lx, 34.50.Fa

I. INTRODUCTION

As recently pointed out [1], low-energy resonance states both above and below the ionization threshold may contribute to dielectronic recombination in astrophysical and laboratory plasmas. Proper inclusion of the below-threshold resonance states can sometimes make substantial changes in the thermally averaged rate coefficients.

The influence of below-threshold resonances on fluorescence has already been observed in Ca^+ [2], and their effect on dielectronic recombination rate coefficients of Mg^{8+} was recently demonstrated theoretically [1]. Since the below-threshold resonance contributions are normally omitted from dielectronic recombination calculations, the experimental verification of their effect on recombination is of paramount importance. One of the aims of this paper is to identify another species that could be used for such experiments.

From a theoretical and experimental standpoint, one of the most widely studied dielectronic recombination rates is associated with the $2s \rightarrow 2p$ excitation in C^{3+}. Precision experiments have been carried out at the CRYRING in Stockholm [3] and the TSR in Heidelberg [4]. The two storage-ring experiments were found to be in good agreement with each other and with high-order relativistic perturbation-theory calculations [3] in regard to resonance structures found just above the ionization threshold.

In this article, we carry out low-order relativistic perturbation-theory calculations for dielectronic recombination cross sections associated with the $2s \rightarrow 2p$ excitation in C^{3+}. Resonance structures arise from the 38 levels of the C^{2+} $1s^22p4l$ configurations that straddle the C^{2+} $1s^22s^2 \rightarrow C^{3+}$ $1s^22s$ ionization threshold. The low-order relativistic calculations are compared with above-threshold storage-ring experiments and map out the below-threshold resonance features.

The remainder of this article is organized as follows. In Sec. II we review low-order relativistic perturbation theory for dielectronic recombination. In Sec. III we apply the perturbative method to calculate dielectronic recombination cross sections associated with the $2s \rightarrow 2p$ excitation in C^{3+}. In Sec. IV we conclude with a summary and an outlook for future work. Unless otherwise stated, all quantities are given in atomic units.

II. THEORY

In the isolated-resonance and independent-processes approximation, the dielectronic recombination cross section for a given N electron initial level i through an intermediate $(N+1)$ electron intermediate level j is given by [5]

$$\sigma_j(\epsilon) = \frac{\pi^2}{|E_{ji}|}\frac{g_j}{2g_i}\frac{\frac{\Gamma_j}{2\pi}}{(\epsilon - E_{ji})^2 + \frac{\Gamma_j^2}{4}}\sum_k A_a(j \rightarrow k)B_j, \quad (1)$$

where E_j is the energy and g_j is the statistical weight of the $(N+1)$ electron doubly excited level, E_i is the energy and g_i is the statistical weight of the N electron initial target level, and $E_{ji} = E_j - E_i$. The branching ratio for radiative stabilization is given by

$$B_j = \frac{\sum_n A_r(j \rightarrow n)}{\sum_k A_a(j \rightarrow k) + \sum_n A_r(j \rightarrow n)}, \quad (2)$$

and the full width at half maximum of the resonance is given by

$$\Gamma_j = \sum_k A_a(j \rightarrow k) + \sum_n A_r(j \rightarrow n), \quad (3)$$

where the radiative A_r and autoionization A_a rates are evaluated using low-order perturbation theory [5]. The electron linear momentum is taken as $k = \sqrt{2|E_{ji}|}$ in the evaluation of the autoionization rates. The strongest radiative rates are to levels that are deeply bound.

For radiative and autoionization rates, the energies and bound state wavefunctions are calculated using a multiconfiguration Dirac-Fock atomic structure code [6]. The continuum state wavefunctions are calculated by solving a single-channel radial Dirac equation, where the Dirac local exchange distorting potential is constructed from Dirac-Fock bound radial orbitals. Resonance energies and rates may also be calculated using the semirelativistic configuration-interaction atomic structure and scattering code AUTOSTRUCTURE [7].

III. RESULTS

Low-order relativistic calculations were carried out for the 28 multiconfiguration levels involving the even-parity configurations: $1s^22s^2$, $1s^22p^2$, $1s^22p4p$, and $1s^22p4f$. Radiative rates were determined for the decay of the 22 even-parity resonance levels to the eight multiconfiguration levels involving the odd-parity configurations: $1s^22s4p$ and $1s^22s4f$, while autoionization rates were determined for the decay of the even-parity resonance levels to the 10 single-configuration levels involving the even-parity configurations:

TABLE I. C^{2+} even-parity resonance-level energies and rates.

Configuration	LSJ level	MCDF energy (eV)	MCDF Auger rate (Hz)	MCDF Radiative rate (Hz)
$1s^22p4p$	$^1P_1$	−0.47	2.9×10^{10}	2.6×10^{8}
	$^3D_1$	−0.38	2.9×10^{11}	2.8×10^{8}
	$^3D_2$	−0.37	2.7×10^{11}	2.8×10^{8}
	$^3D_3$	−0.37	2.2×10^{11}	2.8×10^{8}
	$^3S_1$	−0.22	1.4×10^{14}	3.0×10^{8}
	$^3P_0$	−0.07	5.8×10^{10}	3.2×10^{8}
	$^3P_1$	−0.07	7.1×10^{10}	3.2×10^{8}
	$^3P_2$	−0.06	1.1×10^{9}	3.2×10^{8}
	$^1D_2$	0.20	2.3×10^{13}	3.3×10^{8}
	$^1S_0$	0.64	1.1×10^{15}	3.8×10^{8}
$1s^22p4f$	$^1F_3$	0.37	8.6×10^{10}	2.8×10^{8}
	$^3F_2$	0.38	5.1×10^{8}	2.8×10^{8}
	$^3F_3$	0.38	1.0×10^{11}	2.8×10^{8}
	$^3F_4$	0.38	1.6×10^{11}	2.8×10^{8}
	$^3G_3$	0.48	1.9×10^{14}	3.0×10^{8}
	$^3G_4$	0.49	1.9×10^{14}	3.0×10^{8}
	$^3G_5$	0.49	1.9×10^{14}	3.0×10^{8}
	$^1G_4$	0.53	2.1×10^{14}	3.0×10^{8}
	$^3D_3$	0.54	1.2×10^{12}	3.0×10^{8}
	$^3D_2$	0.54	1.2×10^{12}	3.0×10^{8}
	$^3D_1$	0.54	1.1×10^{12}	3.0×10^{8}
	$^1D_2$	0.57	2.3×10^{12}	3.0×10^{8}

$1s^22s\epsilon s$, $1s^22s\epsilon d$, and $1s^22s\epsilon g$. Low-order relativistic energies for the 22 even-parity resonance levels, relative to the C^{3+} $1s^22s$ configuration, and low-order relativistic autoionization and radiative rates are given in Table I.

Low-order relativistic calculations were also carried out for the 20 multiconfiguration levels involving the odd-parity configurations: $1s^22s2p$, $1s^22p4s$, and $1s^22p4d$. Radiative rates were determined for the decay of the 16 odd-parity resonance levels to the 11 multiconfiguration levels involving the even-parity configurations: $1s^22p^2$, $1s^22s4s$, and $1s^22s4d$, while autoionization rates were determined for the decay of the odd-parity resonance levels to the nine single-configuration levels involving the odd-parity configurations: $1s^22s\epsilon p$, $1s^22s\epsilon f$, and $1s^22s\epsilon h$. Low-order relativistic energies for the 16 odd-parity resonance levels, relative to the C^{3+} $1s^22s$ configuration, and low-order relativistic autoionization and radiative rates are given in Table II.

Low-order semirelativistic calculations were carried out for the 28 configuration-interaction levels involving the even-parity configurations: $1s^22s^2$, $1s^22p^2$, $1s^22p4p$, and

TABLE II. C^{2+} odd-parity resonance-level energies and rates.

Configuration	LSJ level	MCDF energy (eV)	MCDF Auger rate (Hz)	MCDF Radiative rate (Hz)
$1s^22p4s$	$^3P_0$	−1.11	6.1×10^{12}	9.6×10^{8}
	$^3P_1$	−1.11	6.5×10^{12}	9.6×10^{8}
	$^3P_2$	−1.10	6.9×10^{12}	9.6×10^{8}
	$^1P_1$	−0.88	1.2×10^{15}	8.4×10^{8}
$1s^22p4d$	$^1D_2$	0.07	2.6×10^{12}	2.0×10^{9}
	$^3F_2$	0.09	1.9×10^{14}	2.9×10^{8}
	$^3F_3$	0.10	1.9×10^{14}	2.9×10^{8}
	$^3F_4$	0.10	1.9×10^{14}	2.9×10^{8}
	$^3D_1$	0.30	3.0×10^{9}	4.5×10^{9}
	$^3D_2$	0.30	1.2×10^{10}	4.6×10^{9}
	$^3D_3$	0.30	1.2×10^{10}	4.6×10^{9}
	$^3P_2$	0.40	9.4×10^{12}	2.8×10^{9}
	$^3P_1$	0.40	9.6×10^{12}	2.8×10^{9}
	$^3P_0$	0.40	9.8×10^{12}	2.8×10^{9}
	$^1F_3$	0.73	4.3×10^{14}	4.0×10^{9}
	$^1P_1$	0.82	1.5×10^{14}	2.8×10^{9}

TABLE III. C^{2+} even-parity resonance-level energies.

Configuration	LSJ level	MCDF energy (eV)	CIHFR energy (eV)	MBPT energy (eV)	NIST energy (eV)
$1s^2 2p4p$	$^1P_1$	−0.47	−0.47		−0.64
	$^3D_1$	−0.38	−0.39		−0.53
	$^3D_2$	−0.37	−0.38		−0.53
	$^3D_3$	−0.37	−0.38		−0.52
	$^3S_1$	−0.22	−0.24		
	$^3P_0$	−0.07	−0.08		−0.24
	$^3P_1$	−0.07	−0.07		−0.23
	$^3P_2$	−0.06	−0.07		−0.23
	$^1D_2$	0.20	0.17		−0.07
	$^1S_0$	0.64	0.61	0.45	
$1s^2 2p4f$	$^1F_3$	0.37	0.34	0.24	
	$^3F_2$	0.38	0.35	0.24	0.24
	$^3F_3$	0.38	0.35	0.24	0.24
	$^3F_4$	0.38	0.35	0.25	0.25
	$^3G_3$	0.48	0.44	0.35	0.23
	$^3G_4$	0.49	0.45	0.36	0.23
	$^3G_5$	0.49	0.45	0.37	0.23
	$^1G_4$	0.53	0.48	0.38	
	$^3D_3$	0.54	0.49	0.43	0.42
	$^3D_2$	0.54	0.49	0.43	0.43
	$^3D_1$	0.54	0.50	0.44	0.43
	$^1D_2$	0.57	0.52	0.45	

$1s^2 2p4f$, and for the 20 configuration-interaction levels involving the odd-parity configurations: $1s^2 2s2p$, $1s^2 2p4s$, and $1s^2 2p4d$. Low-order semirelativistic energies for the 22 even-parity resonance levels and the 16 odd-parity resonance levels, relative to the C^{3+} $1s^2 2s$ configuration, are given in Tables III and IV (columns labeled CIHFR). Overall the two low-order calculations for the resonance energy levels are in reasonable agreement. Additional low-order semirelativistic calculations for the radiative rates of all the resonance levels and the autoionization rates of the above-threshold resonance levels are in reasonable agreement with the low-order relativistic rates given in Tables I and II, especially for the strongest rates.

Recent high-order relativistic calculations [8] for the positive energy resonance levels of the $1s^2 2p4l$ configurations are given in Tables III and IV (columns labeled MBPT). Energies for 31 of the 38 resonance levels from the NIST atomic spectra database [9] are also given in Tables III and IV (columns labeled NIST). The low-order relativistic and semirelativistic energies for the $1s^2 2p4l$ levels are on average 0.15 eV higher

TABLE IV. C^{2+} odd-parity resonance-level energies.

Configuration	LSJ level	MCDF energy (eV)	CIHFR energy (eV)	MBPT energy (eV)	NIST energy (eV)
$1s^2 2p4s$	$^3P_0$	−1.11	−1.08		−1.24
	$^3P_1$	−1.11	−1.07		−1.23
	$^3P_2$	−1.10	−1.06		−1.22
	$^1P_1$	−0.88	−0.88		
$1s^2 2p4d$	$^1D_2$	0.07	0.10		−0.05
	$^3F_2$	0.09	0.13		−0.05
	$^3F_3$	0.10	0.14		−0.05
	$^3F_4$	0.10	0.14		−0.05
	$^3D_1$	0.30	0.30	0.18	0.18
	$^3D_2$	0.30	0.30	0.18	0.18
	$^3D_3$	0.30	0.30	0.18	0.18
	$^3P_2$	0.40	0.39	0.28	0.28
	$^3P_1$	0.40	0.39	0.29	0.28
	$^3P_0$	0.40	0.39	0.29	0.28
	$^1F_3$	0.73	0.68	0.46	0.31
	$^1P_1$	0.82	0.77	0.58	

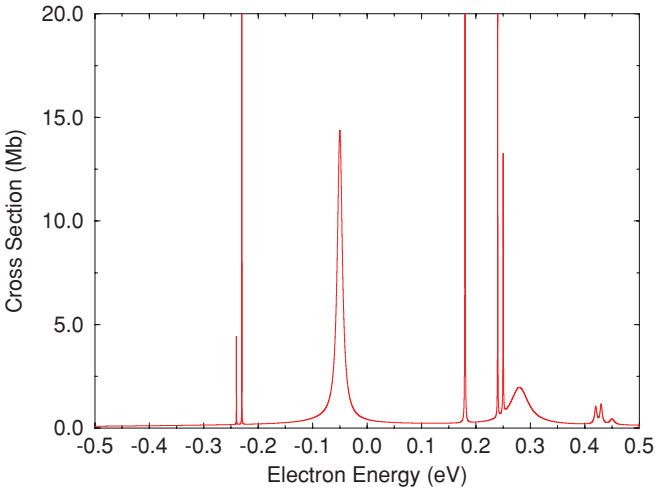

FIG. 1. (Color online) Dielectronic recombination cross sections for C^{3+}. Solid curve: low-order relativistic perturbation-theory calculation (1.0 Mb = 1.0×10^{-18} cm^2).

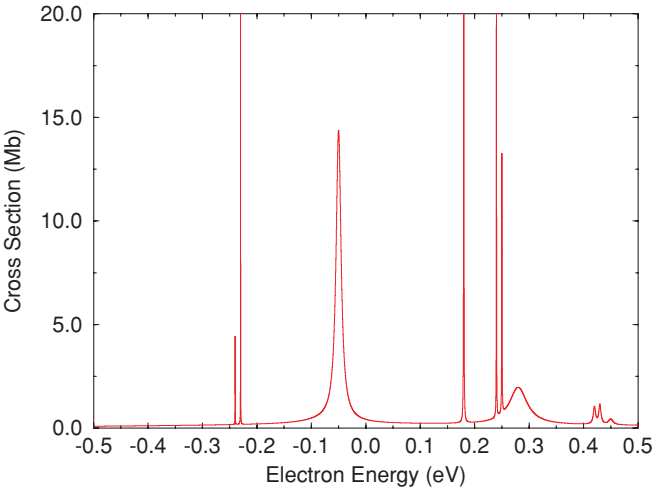

FIG. 2. (Color online) Dielectronic recombination cross sections for C^{3+}. Solid curve: low-order relativistic perturbation-theory calculation folded with a 0.02 eV full width at half maximum Gaussian energy distribution (1.0 Mb = 1.0×10^{-18} cm^2).

than the NIST energies. Overall the high-order relativistic calculations for the above-threshold resonance levels and the NIST energies are in reasonable agreement.

Low-order relativistic calculations for the dielectronic recombination cross sections for C^{3+} are presented in Fig. 1. The energy positions of 31 of the 38 resonance levels have been shifted to agree with the NIST energies, as found in Tables III and IV. For the missing seven NIST energies, five energy positions have been shifted to agree with the high-order relativistic energies. The energy position of the $1s^22p4p\ ^3S_1$ level has been shifted to -0.38 eV, and the energy position of the $1s^22p4s\ ^1P_1$ level has been shifted to -1.01 eV, based on nearby energy shift differences. The strongest resonance features nearest to threshold are the $1s^22p4d\ ^1D_2$ and $^3F_{2,3,4}$ levels at -0.05 eV and the $1s^22p4d\ ^3D_{1,2,3}$ levels at $+0.18$ eV. The strong radiative rate of the $1s^22p4d\ ^1D_2$ level and the strong autoionization rates of the $1s^22p4d\ ^3F_{2,3,4}$ levels yield a high broad feature. The strong radiative rates of the $^3D_{1,2,3}$ levels and their weak autoionization rates yield an extremely high narrow feature. In addition, we have compared the total widths of the resonance levels at -0.05 eV to the spacing of the Rydberg bound levels at this energy, one of the conditions that must be examined for the negative energy resonances to contribute to recombination [1]. We find the total width to be larger than the bound level spacing for the $1s^22p4d\ ^1D_2$ resonance, and the total widths to be an order of magnitude larger than the bound level spacing for the $1s^22p4d\ ^3F_{2,3,4}$ resonances.

To compare with experiment, the low-order relativistic calculations for the dielectronic recombination cross sections for C^{3+} are folded with a 0.02 eV full width at half maximum Gaussian energy distribution and presented in Fig. 2. Above threshold the convoluted resonance features are in moderately good agreement with those observed by the two storage-ring experiments [3,4] and those predicted by high-order relativistic calculations [3]. The main difference is around 0.25 eV, where the experiments observe and the high-order relativistic calculations predict a more asymmetrical double-hump feature. Below threshold the low-order relativistic calculations predict the resonance feature at -0.05 eV to have almost half the strength of the large resonance feature at $+0.18$ eV.

IV. SUMMARY

Low-order relativistic perturbation theory has been applied to calculate the dielectronic recombination in C^{3+} above and below the ionization threshold. Resonances attributed to the $1s^22p4l$ configurations straddle the threshold, with a strong resonance feature found at -0.05 eV. Certainly an exotic plasma in which a C^{3+} atomic ion finds itself surrounded by very low-energy electrons would have its dielectronic recombination rate strongly influenced by the $1s^22p4d\ ^1D,^3F$ resonances. With the continued experimental development of new ways to trap atomic ions [10], the present calculations provide a guide for future measurements of the contribution made by below-threshold resonances to recombination in plasmas.

ACKNOWLEDGMENTS

This work was supported in part by grants from the US Department of Energy and the US National Science Foundation. Computational production work was carried out at the National Energy, and computational production work was carried out at the National Energy Research Scientific Computing Center in Oakland, California, and the National Institute for Computational Sciences in Knoxville, Tennessee.

[1] F. Robicheaux, S. D. Loch, M. S. Pindzola, and C. P. Ballance, Phys. Rev. Lett. **105**, 233201 (2010).

[2] S. D. Bergeson and F. Robicheaux, Phys. Rev. Lett. **101**, 073202 (2008).

[3] S. Mannervik, D. DeWitt, L. Engstrom, J. Lidberg, E. Lindroth, R. Schuch, and W. Zong, Phys. Rev. Lett. **81**, 313 (1998).
[4] S. Schippers, A. Muller, G. Gwinner, J. Linkemann, A. A. Saghiri, and A. Wolf, Astrophys. J. **555**, 1027 (2001).
[5] M. S. Pindzola and N. R. Badnell, Phys. Rev. A **42**, 6526 (1990).
[6] I. P. Grant, *Relativistic Quantum Theory of Atoms and Molecules* (Springer, New York, 2007).
[7] N. R. Badnell, J. Phys. B **30**, 1 (1997).
[8] A. Derevianko, V. A. Dzuba, and M. G. Kozlov, Phys. Rev. A **82**, 022720 (2010).
[9] [http://physics.nist.gov/PhysRefData] (2010).
[10] M. Hobein, A. Solders, M. Suhonen, Y. Liu, and R. Schuch, Phys. Rev. Lett. **106**, 013002 (2011).